AGU PUBLICATIONS

Geophysical Research Letters

RESEARCH LETTER
10.1002/2015GL066390

Key Points:
- Clear core phases are extracted across the entire USArray using earthquake coda interferometry
- A strong N-S trending travel time anomaly is observed across the central U.S.
- An inner core hemispherical model with boundaries at longitude 99 W and 88E is proposed

Supporting Information:
- Texts S1–S4 and Figures S1–S8

Correspondence to:
H.-H. Huang,
HsinHua.Huang@utah.edu

Citation:
Huang, H.-H., F.-C. Lin, V. C. Tsai, and K. D. Koper (2015), High-resolution probing of inner core structure with seismic interferometry, *Geophys. Res. Lett.*, *42*, 10,622–10,630, doi:10.1002/2015GL066390.

Received 29 SEP 2015
Accepted 5 DEC 2015
Accepted article online 9 DEC 2015
Published online 23 DEC 2015

High-resolution probing of inner core structure with seismic interferometry

Hsin-Hua Huang[1,2], Fan-Chi Lin[1], Victor C. Tsai[2], and Keith D. Koper[1]

[1]Department of Geology and Geophysics, University of Utah, Salt Lake City, Utah, USA, [2]Seismological Laboratory, California Institute of Technology, Pasadena, California, USA

Abstract Increasing complexity of Earth's inner core has been revealed in recent decades as the global distribution of seismic stations has improved. The uneven distribution of earthquakes, however, still causes a biased geographical sampling of the inner core. Recent developments in seismic interferometry, which allow for the retrieval of core-sensitive body waves propagating between two receivers, can significantly improve ray path coverage of the inner core. In this study, we apply such earthquake coda interferometry to 1846 USArray stations deployed across the U.S. from 2004 through 2013. Clear inner core phases $PKIKP^2$ and $PKIIKP^2$ are observed across the entire array. Spatial analysis of the differential travel time residuals between the two phases reveals significant short-wavelength variation and implies the existence of strong structural variability in the deep Earth. A linear N-S trending anomaly across the middle of the U.S. may reflect an asymmetric quasi-hemispherical structure deep within the inner core with boundaries of 99°W and 88°E.

1. Introduction

In recent decades, increasingly complex models have been proposed for the structure and dynamics of Earth's inner core (for reviews see *Deuss* [2014] and *Tkalčić* [2015]). Features of these models include differential rotation of the inner core [*Song and Richards*, 1996; *Zhang et al*., 2005; *Tkalčić et al*., 2013], the existence of fine-scale (~1–10 km) heterogeneities [*Vidale and Earle*, 2000; *Koper et al*., 2004; *Peng et al*., 2008], a distinct innermost inner core [*Ishii and Dziewonski*, 2002; *Cao and Romanowicz*, 2007; *Niu and Chen*, 2008; *Wang et al*., 2015], and a long-wavelength quasi-hemispherical structure [*Tanaka and Hamaguchi*, 1997; *Niu and Wen*, 2001; *Deuss et al*., 2010; *Lythgoe et al*., 2014].

Many of these models, which are still debated, can be tested and refined as the distribution of seismic stations around the globe continues to improve; however, the uneven distribution of earthquakes places fundamental limits on the geographical sampling of the inner core. Moreover, in order to mitigate the effects of mantle heterogeneity and source mislocation, many body wave studies of the inner core measure the arrival time of PKIKP (PKPdf) with respect to a reference phase that only traverses the mantle and outer core (PKPcd, PKPbc, and PKPab), which tends to limit coverage mostly to the top ~300 km of the inner core, i.e., to the outer parts of the inner core (OIC).

New developments in seismic interferometry, however, may provide the means to overcome the limitations in lateral and radial sampling of the inner core that are common to many previous earthquake based studies. Several authors have recently shown that body waves that propagate deep within the Earth can be extracted by cross correlation of either ambient noise or earthquake coda [*Poli et al*., 2012; *Boue et al*., 2013; *Lin et al*., 2013; *Nishida*, 2013; *Boue et al*., 2014]. These techniques potentially provide sensitivity to any desired ray path across the inner core between two receivers, as long as the used diffusive waves well sample the stationary phase region [*Snieder*, 2004; *Ruigrok et al*., 2008; *Fan and Snieder*, 2009]. Importantly, uncertainties related to earthquake location are eliminated, which may prove especially fruitful for studies of time-dependent inner core structure.

Most recently, *Wang et al*. [2015] analyzed the autocorrelation of earthquake coda recorded by globally distributed arrays of broadband seismometers to extract the inner core body wave phases $PKIKP^2$ (also known as P'dfP'df) and $PKIIKP^2$, which take off from a station, reflect at the farside of the Earth's surface and then propagate back to the same station. For this phase pair, the major difference in ray path exists within the inner core where $PKIKP^2$ propagates directly through the center of the Earth, while $PKIIKP^2$ mainly traverses the OIC with underside reflections at the inner core boundary (ICB) (Figure 1a). By analyzing the global variation of differential times between these two phases, *Wang et al*. [2015] proposed a distinct seismic

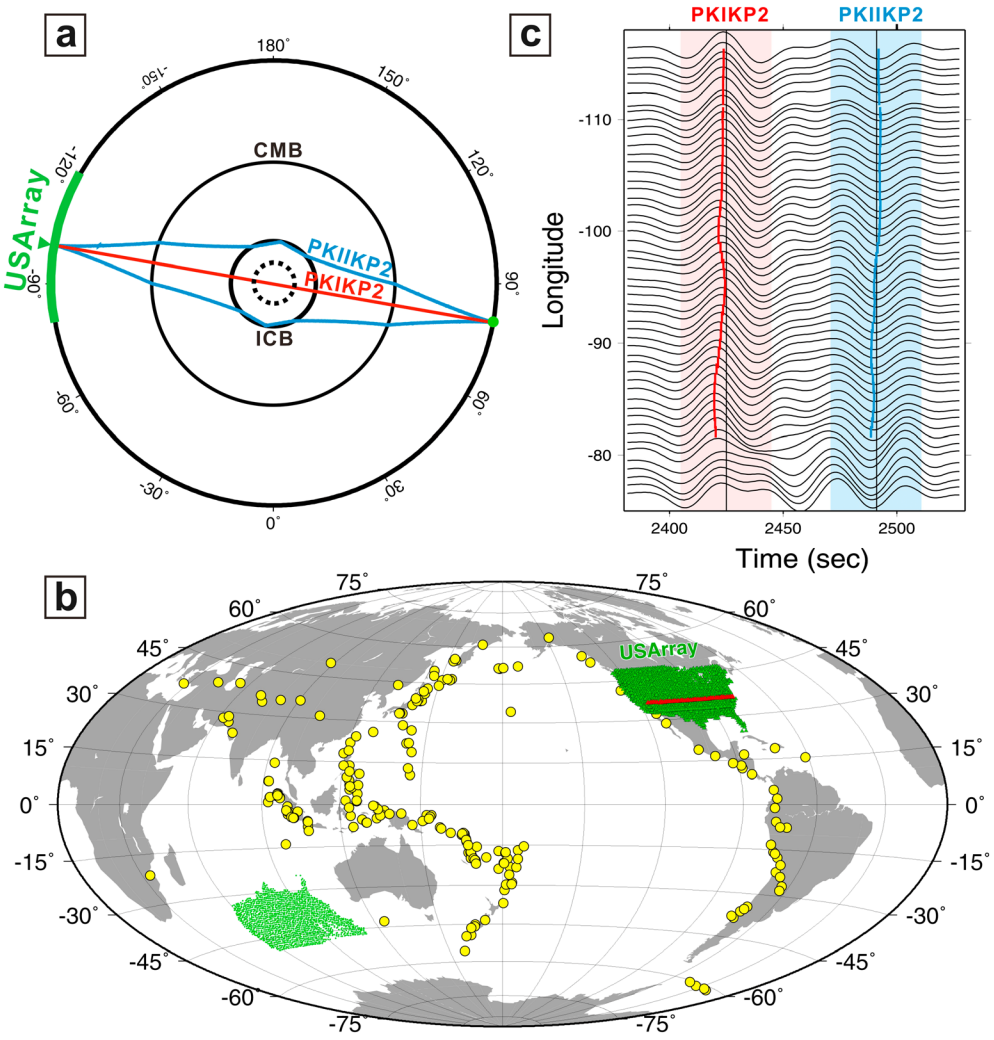

Figure 1. Illustration of the data used in this study. (a) Ray paths of extracted PKIKP^2 and PKIIKP^2 phases. Green line and dots demonstrate the aperture of USArray as well as the antipodal bounce points (Figure 1b). (b) Distribution of $M_W \geqq 7.0$ earthquakes (yellow dots) and USArray stations (green triangles). Green dots denote the antipodes of USArray stations. (c) Extracted Green's functions along a linear station array denoted by the red triangles in Figure 1b. The time window used for travel time measurement and the measured time residuals are marked by the shaded zone and vertical bars for the phase PKIKP^2 (red) and for the phase PKIIKP^2 (blue).

anisotropy in the innermost inner core of ~600 km radius with a fast axis near the equatorial plane through Central America and Southeast Asia. The PKIKP^2-PKIIKP^2 phase pair samples the entire inner core (not just the OIC) and therefore has great potential to complement earthquake generated body wave methods.

In this study we apply earthquake coda interferometry techniques [*Lin et al.*, 2013; *Lin and Tsai*, 2013; *Wang et al.*, 2015] to 1846 USArray stations deployed across North America from January 2004 through September 2013 (Figure 1b) to extract differential travel times of PKIKP^2 and PKIIKP^2. Its dense station spacing, high quality recordings (e.g., uniform instrumentation), and especially its wide aperture make USArray an ideal network to probe the deep Earth with seismic interferometry. Its location straddling a recently proposed inner core hemisphere boundary at 95°W [*Lythgoe et al.*, 2014] also provides a good opportunity to evaluate that model.

Although most USArray stations were operational for just 18–24 months, we demonstrate that reliable PKIKP^2 and PKIIKP^2 signals can be extracted at most stations and used to derive high-resolution maps of travel time residuals. We then validate the observed short-wavelength variations and discuss the implications for structure in the deep Earth.

2. Data and Methods

We mainly follow the method described by *Lin and Tsai* [2013] to obtain vertical-vertical cross-correlation functions (CCF) and autocorrelation functions (ACF) using coda energy between 20,000 and 40,000 s after the origin time of earthquakes with moment magnitudes larger than 7.0 for all available station pairs among the 1846 USArray stations (Figure 1b). This method first uses a running absolute mean over a 128 s time window of the 15–50 s bandpassed raw coda waveform for temporal normalization to suppress impulsive high-amplitude earthquake signals. The amplitude spectrum between periods of 5 and 800 s of the normalized coda waveforms is then flattened before cross correlation. While the temporal normalization process may suppress the amplitude of earthquake coda to the ambient noise level, no further processing is used to reduce earthquake contributions. In the end, a total of 143 $M_w \geq 7.0$ earthquakes are used. For each station, which records about 20–30 large earthquakes within its ~2 years operational time period, the vertical component of large earthquake coda are cross correlated and stacked to extract body wave signals.

Typically 20–30 events are not sufficient to obtain high signal-to-noise ratios (SNRs) in the correlations. *Wang et al*. [2015] used a similar number of earthquakes but required additional stacking over all of the stations in each array. For this reason, we perform a neighborhood stacking method to enhance the signal, in which all the ACFs and CCFs within a given radius are further slant-stacked. This operation results in a final neighborhood-stacked ACF (NACF) that stacks the number of sources equivalent to $\overline{Ne} \times Ns$, where Ns is the number of stacked station pairs within the given radius and $\overline{Ne}$ is the average number of large earthquakes that were recorded by the station pairs included in the stack. The SNR is then calculated by taking the maximum amplitude of the desired phase ($PKIKP^2$ or $PKIIKP^2$) and dividing by the root-mean-square amplitude of the noise for a time period (1100–2300 s) in which no known physical phases arrive (Figure S2 in the supporting information).

The neighborhood radius is a free parameter that is varied and tested in Text S1.1. In general, larger radii not only lead to cleaner waveforms but also lower the spatial resolution since the travel time information at each station are averaged by more neighboring stations. A 300 km stacking radius is selected as a compromise between the phase SNR and the structural resolution (Text S1.1). With a radius of 300 km, the NACF yields a stack equivalent to the averaging of about 30,000 sources (Figure S1). After all the NACFs are computed and resampled to 10 samples per second, we apply an adaptive stacking method [*Jansson and Husebye*, 1966; *Rawlinson and Kennett*, 2004] to a 40 s time window centered at the predicted time from *ak135* [*Kennett et al*., 1995] to measure the relative travel time residuals for $PKIKP^2$ and $PKIIKP^2$, respectively (Figures 1a and 1c). The differential travel time residuals between $PKIKP^2$ and $PKIIKP^2$ are then calculated and used to constrain inner core structure (Figure 2).

While some coda-derived CCF travel time measurements may be biased by anisotropic source distributions [*Boue et al*., 2014], the NACF travel time measurements derived here are less likely to be biased because neighborhood stacking integrates station pairs over all azimuths. Based on an uncertainty test described in Text S1.2, for the NACFs with SNR greater than 3 and cross-correlation coefficients (CC) greater than 0.96, we estimate (one standard deviation) uncertainties of 0.46 s and 0.33 s for $PKIKP^2$ and $PKIIKP^2$, respectively.

3. Results and Discussion

3.1. $PKIKP^2$ and $PKIIKP^2$ Measurements

Travel time residuals for $PKIKP^2$, $PKIIKP^2$, and $PKIKP^2$-$PKIIKP^2$ are shown in Figure 2. NACFs that do not fulfill the selection criterion (SNR ≥ 3 and CC ≥ 0.96) are excluded. In general, almost all $PKIKP^2$ measurements meet the selection criterion except those made near the east coast of the U.S. where the stations had operated for only about 9 months at the time this study was conducted. In contrast, there are fewer measurements for $PKIIKP^2$, since it is usually a weaker phase.

Clearly, the two phases display different residual variations. $PKIIKP^2$, which mainly samples the mantle and OIC, exhibits positive travel time residuals (delayed arrivals) to the west and the negative residuals (advanced arrivals) to the east, with a boundary roughly at 100°W (Figures 2a and 2d). $PKIKP^2$, which traverses the very center of the Earth, shows a similar east-west pattern but with the boundary shifted in longitude to 90°W. It also shows a roughly circular fast anomaly (advanced arrivals) beneath Montana (~47°N, 110°W) (Figures 2b and 2e). Taking the difference between the two phases enhances the Montana fast anomaly to around −4 s

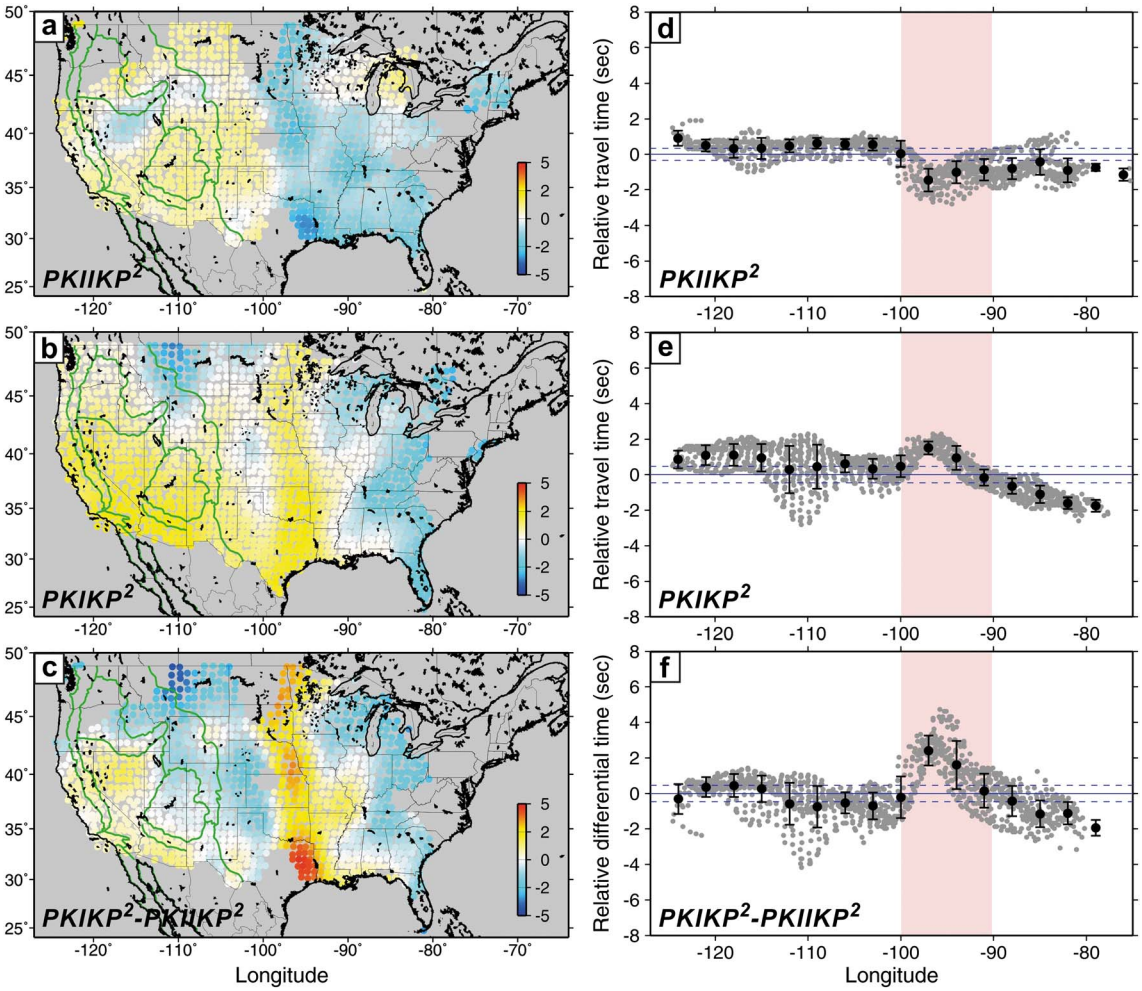

Figure 2. Relative travel time residuals of (a–c) $PKIKP^2$, $PKIIKP^2$, and $PKIKP^2$-$PKIIKP^2$ in map view and as a function of (d–f) longitude. The delayed (positive) and advanced (negative) time residuals are color coded in map view and indicated by gray dots in the scatterplots. The black dots and bars denote the mean and the one standard deviation time residuals binned each 3°. Blue dashed lines show the estimated data uncertainty from the odd/even test (Text S1.2). A zone of prominent delayed time residuals of $PKIKP^2$-$PKIIKP^2$ is marked by the red shaded zone (Figures 2d–2f).

and results in a prominent N-S trending slow anomaly (delayed arrivals) across the middle of the U.S., with an average value of 2.5 s (Figures 2c and 2f). Note that the strong (4 s) positive $PKIKP^2$-$PKIIKP^2$ spot at the southern end of the N-S trending anomaly is primarily related to a fast spot in $PKIIKP^2$ measurements. Since $PKIKP^2$ and $PKIIKP^2$ are round trip (reflected) phases, this implies one-way travel time residuals of −2 s and 1.25 s for the Montana and the N-S trending anomalies, respectively. Moreover, we also use an integrated 3-D velocity model, instead of the $PKIIKP^2$ reference phase, to correct the $PKIKP^2$ observations (Text S2) and find that the corrected $PKIKP^2$ residuals still clearly show the Montana and N-S trending anomalies (Figure S5).

3.2. Location of Anomalies

Differential travel time residuals for PKIKP-PKIIKP and $PKIKP^2$-$PKIIKP^2$ have previously been mapped to the inner core, where the ray paths in the phase pairs separate the most [*Niu and Chen*, 2008; *Wang et al.*, 2015]. However, the separation of the ray paths in the lowermost mantle is also notable (Figure 1a). To investigate whether the observed anomaly (Figure 2) could result from lowermost mantle structure, we conduct a finite-frequency analysis in Text S3 using a single scattering Born approximation [*Dahlen et al.*, 2000] and find that for the long-period (20–50 s) data used here; the sensitivity radius (i.e., the radius of the first Fresnel zone along the ray path) is ~900 km for $PKIKP^2$ and ~1500 km for $PKIIKP^2$ at a depth of 2890 km (lowermost mantle), and these sensitivities thus highly overlap each other beneath USArray (Figures S6 and S7); however,

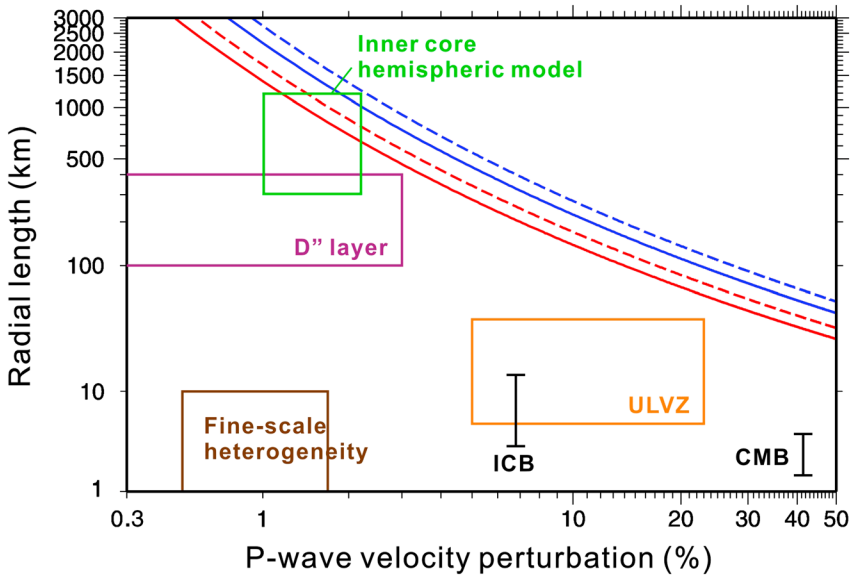

Figure 3. Relationship between *P* wave velocity (V_P) perturbation and radial length scale (i.e., thickness/height) of deep earth structures. Red solid and dotted curves represent the relationships for a slow V_P anomaly (1.25 s time residual) in the inner core and the lowermost mantle; blue solid and dotted curves represent the relationships for a fast V_P anomaly (−2 s time residual) in the inner core and the lowermost mantle according to equation (1). The ranges of the V_P perturbation and length scale for the D″ layer, ultralow velocity zone (ULVZ), fine-scale heterogeneity, topography variations of inner core boundary (ICB) and core-mantle boundary (CMB), and inner core hemispheric model are denoted by vertical black bars and boxes in different colors, respectively. Axes have logarithmic scales. Refer to section 3.3 for more details.

the sensitivity radius of $PKIIKP^2$ (~4000 km) is much wider than that of $PKIKP^2$ (~950 km) on the farside of the Earth. This suggests that lowermost mantle structure, such as D″ anomalies or ultralow velocity zones [*McNamara et al.*, 2010], beneath the USArray are unlikely to contribute to the observed travel time anomalies of $PKIKP^2$-$PKIIKP^2$, but structure on the farside of Earth (beneath the Indian Ocean), that is, sampled by the wider sensitivity of $PKIIKP^2$ but not as much by $PKIKP^2$ may potentially be mapped into the differential time residuals.

3.3. Amplitude of Anomalies

To explain such large travel time residuals of −4 s and 2.5 s (−2 s and 1.25 s one way) for the Montana fast anomaly and the N-S trending slow anomaly, one needs an anomaly that is either strong in *P* wave velocity (V_P) change or large in radial length scale (i.e., the length of ray traveling through the anomaly) in the inner core or at the farside lowermost mantle, or alternatively with large topography at the ICB or core-mantle boundary (CMB). A trade-off relationship between the length scale and velocity change of a given anomaly can be expressed as

$$dt = -\left(\frac{dv}{v}\right)\frac{l}{v}, \tag{1}$$

where dt is the observed travel time anomaly, v is the background V_P, $\frac{dv}{v}$ is the percentage change in velocity for the anomaly, and l represents the radial length scale of the anomaly. Substituting the average V_P of the inner core (11.15 km/s) [*Kennett et al.*, 1995] for v and the observed 1.25 s residual (NS-trending anomaly) for dt into equation (1), we can obtain a trade-off curve that represents how large of a length scale and how slow of a V_P anomaly would be needed in the inner core (red solid curve) to produce a 1.25 s residual (Figure 3). Likewise, a trade-off curve that represents a slow anomaly in the lowermost mantle can be obtained by replacing the V_P of the inner core with that of the lowermost mantle (13.6 km/s) (red dashed curve). In a similar manner, trade-off curves for the −2 s residual Montana anomaly are calculated.

To explore what structure could match the trade-off curves, we summarize the radial length scales and V_P perturbations of various deep Earth structures in Figure 3, including small-scale ICB variations (3–14 km),

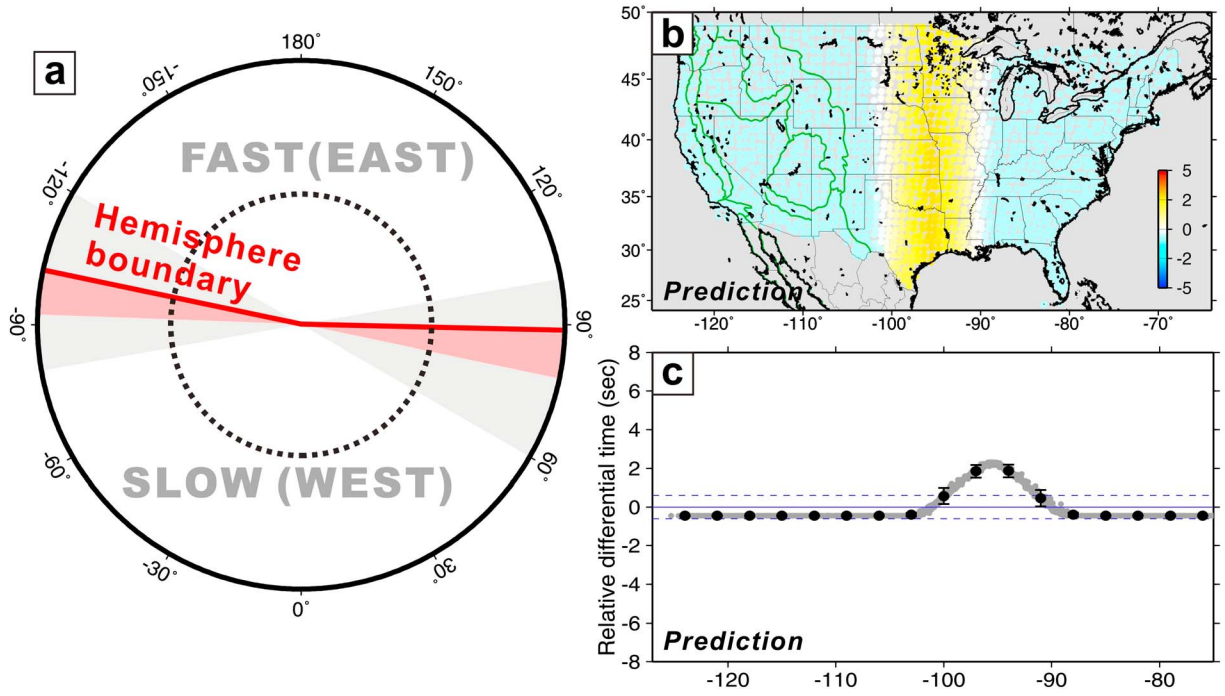

Figure 4. Models and predictions for observed travel time anomalies. (a) A hemispheric model proposed for the N-S trending slow anomaly between −90° and −100° (90–100°W). Gray and red shaded zones indicate the sampling areas of $PKIKP^2$ for the entire USArray and the anomalous positive residual zones in longitude, respectively. The predicted relative travel time residuals of the hemispheric model (Figure 4a) are shown (b) in map view and (c) in longitude. For the calculation of predictions, refer to Text S4. An asymmetric hemispheric model with a larger slow-velocity hemisphere (eastern hemisphere) and two boundaries at longitudes of 99°W and 88°E can readily reproduce the observed N-S trending anomaly across the middle of the U.S. (Figure 2). The black dots and bars denote the mean and the one standard deviation time residuals binned each 3°. Blue dashed lines show the estimated data uncertainty from the odd/even test (Text S1.2).

fine-scale inner core heterogeneity (1–10 km wavelengths with ~1.0–2.0% V_P variations), lowermost mantle D″ structure (thickness of 100–400 km and ±3% V_P variations), ultralow velocity zones (5–23% V_P drops and 5–40 km thicknesses), long-wavelength CMB variations (±1.5–4 km), and inner core hemispherical models (1.0–2.2% V_P differences between two hemispheres at the latitude of USArray and model radii that range from 300 km to the entire inner core) [*Ishii and Dziewonski*, 2002; *Song and Dai*, 2008; *Dai et al*., 2012; *Vidale and Earle*, 2000; *Koper et al*., 2004; *Cobden and Thomas*, 2013; *Yao et al*., 2015; *Rondenay and Fischer*, 2003; *McNamara et al*., 2010; *Brown et al*., 2015; *Garcia and Souriau*, 2000; *Sze and van der Hilst*, 2003; *Irving and Deuss*, 2011; *Yee et al*., 2014; *Lythgoe et al*., 2014]. We observe that except for the inner core hemispherical model, all other structures generally under predict the amplitude of the $PKIKP^2$-$PKIIKP^2$ residuals.

3.4. Inner Core Hemispherical Model

Over the past two decades, the number of observations of quasi-hemispherical inner core structure has increased significantly [*Tanaka and Hamaguchi*, 1997; *Creager*, 1999; *Niu and Wen*, 2001; *Garcia*, 2002; *Irving and Deuss*, 2011; *Lythgoe et al*., 2014]. Previous studies have suggested that the quasi-western hemisphere in the inner core is more anisotropic and has a lower isotropic V_P than the quasi-eastern hemisphere [*Irving and Deuss*, 2011; *Deuss*, 2014; *Yee et al*., 2014; *Lythgoe et al*., 2014], with the V_P of the western hemisphere being about 1.0–2.2% slower than that of eastern hemisphere at USArray latitudes (30–50°N). Assuming such a hemispherical model of the entire inner core (1217 km), we find that a larger quasi-western hemisphere bisected by two boundaries at 99°W and 88°E that is ~1.2% slower than the quasi-eastern one can readily reproduce both the residual amplitudes and the linear geometry of our observed N-S trending anomaly (Figure 4 and Text S4). Because the derived $PKIKP^2$ phase here is zero offset, it traverses the center of Earth and is quite sensitive to the longitude of the hemisphere boundary; the $PKIIKP^2$ phase, on the other hand, only sweeps through the OIC and is therefore insensitive to the boundary. A larger hemisphere with slower V_P would create a delayed arrival time zone where $PKIKP^2$ travels only through the slower hemisphere but elsewhere travels through both hemispheres (red shaded area in Figure 4a).

Theobserved zone width would then be proportional to the exterior angles of the two hemisphere boundaries. Based on this model, the gradual residual change across two boundaries (Figure 2) can result from the neighborhood stacking method we employed (Figure 4c and Text S4) and also the finite-frequency effect of data.

The 1.2% V_P difference that is required in our model is in good agreement with the 1.0–2.2% reported in previous studies. Furthermore, the 99°W western boundary constrained in this study is similar to the 95°W boundary proposed by *Lythgoe et al*. [2014], though dissimilar to the 151°W–160°E range reported in other studies [*Tanaka and Hamaguchi*, 1997; *Creager*, 1999; *Niu and Wen*, 2001; *Garcia*, 2002; *Irving and Deuss*, 2011]. In contrast, our boundary at 88°E is different from the 14°–60°E range previously proposed [*Tanaka and Hamaguchi*, 1997; *Creager*, 1999; *Niu and Wen*, 2001; *Garcia*, 2002; *Irving and Deuss*, 2011; *Lythgoe et al*., 2014]. However, it is worth noting that our 88°E eastern boundary still lies within the uncertainty range of the eastern hemisphere boundaries of *Irving and Deuss* [2011] and *Lythgoe et al*. [2014]. The discrepancy in boundary location could arise from different sensitivities in the data sets used by various authors. The $PKIKP^2$-$PKIIKP^2$ and direct PKIKP data used here and in *Lythgoe et al*. [2014] are sensitive to the entire inner core, while the PKPbc-PKIKP or PKPab-PKIKP data used in all other studies are mainly sensitive to OIC structure. Considering the possible depth dependence of the inner core quasi-hemisphere boundaries [*Waszek et al*., 2011; *Waszek and Deuss*, 2011], the boundary locations proposed in this study (and in *Lythgoe et al*. [2014]) may imply an orientation of hemisphere boundaries of the inner parts of the inner core distinct from that of the well-documented OIC. If true, and assuming a 900 km radius (excluding the OIC) or 600 km radius (for just the innermost inner core of, e.g., *Wang et al*. [2015]) for our hemispherical model, our results would then require a 1.5% or 2.3% V_P difference between the two hemispheres, respectively.

The possibility of contamination from lower mantle anomalies, such as from D'' or ultralow velocity zones (ULVZs), cannot be completely ruled out by our data set. In particular, the circular (not linear) fast anomaly beneath Montana cannot be explained by an inner core hemispherical model and more likely reflects a localized D'' anomaly beneath the Indian Ocean. This D'' anomaly would then require either a thickness over 700 km or a V_P change over 5% to have a residual of −2 s (Figure 3), although the −2 s residual could be closer to −1.5 s if the correction using a 3-D velocity model accounts for mantle structure more accurately than using $PKIIKP^2$ (Text S4 and Figure S5). In addition to the first-order features such as the Montana and N-S trending anomalies, the weaker, local variations especially in the western U.S. (Figure 2) may indicate the existence of local-scale (few hundred kilometers) heterogeneity in the inner core [*Ohtaki et al*., 2012; *Yee et al*., 2014] or the lowermost mantle [*McNamara et al*., 2010].

4. Concluding Remarks

This study is the first to obtain such dense sampling of inner core structure with seismic interferometry. The successful extraction of coherent and reliable body wave signals from earthquake coda interferometry is encouraging and suggests that the method can be used with other wide aperture arrays such as those in China and Europe to probe the deep Earth at different locations. The antipodal-distance measurements of $PKIKP^2$ and $PKIIKP^2$ obtained here are rare in earthquake generated body wave data sets and are critical to constrain the structure at the very center of the Earth [*Rial and Cormier*, 1980]. Moreover, *Cormier* [2015] recently showed that the waveforms of near antipodal PKIIKP could be used to detect inner core solidification, and the waveforms of extracted antipodal $PKIIKP^2$ should have similar sensitivities. Integrating these new interferometry data with traditional earthquake data to provide better sampling of the entire inner core would be a subject of great importance.

Most importantly, the high-resolution travel time image derived in this study displays short-wavelength variations in $PKIKP^2$-$PKIIKP^2$ travel time residuals, which imply strong, complex structural variability in the deep Earth. The linear and large (1.25 s) N-S trending anomaly across the center of the U.S. suggests the need for an asymmetric quasi-hemispherical structure in the inner parts of the inner core. Since potential contamination resulting from lower mantle structure beneath the Indian Ocean may exist, more stations for seismic interferometry, such as in Canada and South America, would be particularly useful in further investigating the extension of the N-S trending anomaly.

Acknowledgments
We thank Alex Song for helpful discussion. We also thank H. Tkalcic and an anonymous reviewer for their constructive comments. All waveform data used in this study can be downloaded from the IRIS Data Management Center. This work was supported by National Science Foundation grants EAR-1316348 and CyberSEES-1442665, the King Abdullah University of Science and Technology (KAUST) under award OCRF-2014-CRG3-2300, and the Ministry of Science and Technology, Taiwan, grant 104-2917-I-564-052.

References

Boue, P., P. Poli, M. Campillo, H. Pedersen, X. Briand, and P. Roux (2013), Teleseismic correlations of ambient seismic noise for deep global imaging of the Earth, *Geophys. J. Int.*, *194*, 844–848.

Boue, P., P. Poli, M. Campillo, and P. Roux (2014), Reverberations, coda waves and ambient noise: Correlations at the global scale and retrieval of the deep phases, *Earth Planet. Sci. Lett.*, *391*, 137–145.

Brown, S. P., M. S. Thorne, L. Miyagi, and S. Rost (2015), A compositional origin to ultralow-velocity zones, *Geophys. Res. Lett.*, *42*, 1039–1045, doi:10.1002/2014GL062097.

Cao, A., and B. Romanowicz (2007), Test of the innermost inner core models using broadband PKIKP travel time residuals, *Geophys. Res. Lett.*, *34*, L08303, doi:10.1029/2007GL029384.

Cobden, L., and C. Thomas (2013), The origin of D″ reflections: A syatematic study of seismic array data sets, *Geophys. J. Int.*, *194*, 1091–1118.

Cormier, V. F. (2015), Detection of inner core solidification from observations of antipodal PKIIKP, *Geophys. Res. Lett.*, *42*, 7459–7466, doi:10.1002/2015GL065367.

Creager, K. C. (1999), Large-scale variations in inner core anisotropy, *J. Geophys. Res.*, *104*, 23,127–23,139.

Dahlen, F. A., S.-H. Hung, and G. Nolet (2000), Frechet kernels for finite-frequency traveltimes–I. Theory, *Geophys. J. Int.*, *141*, 157–174.

Dai, W., W. Wang, and L. Wen (2012), Irregular topography at the Earth's inner core boundary, *Proc. Natl. Acad. Sci. U.S.A.*, *109*, 7654–7658.

Deuss, A. (2014), Heterogeneity and anisotropy of Earth's inner core, *Annu. Rev. Earth Planet. Sci.*, *42*, doi:10.1146/annurev-earth-060313-054658.

Deuss, A., J. C. E. Irving, and J. H. Woodhouse (2010), Regional variation of inner core anisotropy from seismic normal mode observations, *Science*, *328*, doi:10.1126/science.1188596.

Fan, Y., and R. Snieder (2009), Required source distribution for interferometry of waves and diffusive fields, *Geophys. J. Int.*, *179*, 1232–1244.

Garcia, R. (2002), Constraints on upper inner-core structure from waveform inversion of core phases, *Geophys. J. Int.*, *150*, 651–664.

Garcia, R., and A. Souriau (2000), Amplitude of the core–mantle boundary topography estimated by stochastic analysis of core phases, *Phys. Earth Planet. Inter.*, *117*, 345–359.

Irving, J. C. E., and A. Deuss (2011), Hemispherical structure in inner core velocity anisotropy, *J. Geophys. Res.*, *116*, B04307, doi:10.1029/2010JB007942.

Ishii, M., and A. M. Dziewonski (2002), The innermost inner core of the earth: Evidence for a change in anisotropic behavior at the radius of about 300 km, *Proc. Natl. Acad. Sci. U.S.A.*, *99*, 14,026–14,030.

Jansson, B., and E. S. Husebye (1966), Application of array data techniques to a network of ordinary seismograph stations, *Pure Appl. Geophys.*, *63*, 83–104.

Kennett, B. L. N., E. R. Engdahl, and R. Buland (1995), Constraints on seismic velocities in the Earth from traveltimes, *Geophys. J. Int.*, *122*, 108–124.

Koper, K. D., J. M. Franks, and M. Dombrovskaya (2004), Evidence for small-scale heterogeneity in Earth's inner core from a global study of PKiKP coda waves, *Earth Planet. Sci. Lett.*, *228*, 227–241.

Lin, F.-C., and V. C. Tsai (2013), Seismic interferometry with antipodal station pairs, *Geophys. Res. Lett.*, *40*, 4609–4613, doi:10.1002/grl.50907.

Lin, F.-C., V. C. Tsai, B. Schmandt, Z. Duputel, and Z. Zhan (2013), Extracting seismic core phases with array interferometry, *Geophys. Res. Lett.*, *40*, doi:10.1002/grl.50237.

Lythgoe, K. H., A. Deuss, J. F. Rudge, and J. A. Neufeld (2014), Earth's inner core: Innermost inner core or hemispherical variations?, *Earth Planet. Sci. Lett.*, *385*, 181–189.

McNamara, A. K., E. J. Garnero, and S. Rost (2010), Tracking deep mantle reservoirs with ultra-low velocity zones, *Earth Planet. Sci. Lett.*, *299*, 1–9.

Nishida, K. (2013), Global propagation of body waves revealed by cross-correlation analysis of seismic hum, *Geophys. Res. Lett.*, *40*, 1691–1696, doi:10.1002/grl.50269.

Niu, F., and L. Wen (2001), Hemispherical variations in seismic velocity at the top of the Earth's inner core, *Nature*, *410*, 1081–1084.

Niu, F., and Q.-F. Chen (2008), Seismic evidence for distinct anisotropy in the innermost inner core, *Nat. Geosci.*, *1*, doi:10.1038/ngeo314.

Ohtaki, T., S. Kaneshima, and K. Kanjo (2012), Seismic structure near the inner core boundary in the south polar region, *J. Geophys. Res.*, *117*, B03312, doi:10.1029/2011JB008717.

Peng, Z., K. D. Koper, J. E. Vidale, F. Leyton, and P. Shearer (2008), Inner-core fine-scale structure from scattered waves recorded by LASA, *J. Geophys. Res.*, *113*, B09312, doi:10.1029/2007JB005412.

Poli, P., M. Campillo, H. Pedersen, and L. A. P. N. E. T. Working Group (2012), Body-wave imaging of Earth's mantle discontinuities from ambient seismic noise, *Science*, *338*, doi:10.1126/science.1228194.

Rawlinson, N., and B. L. N. Kennett (2004), Rapid estimation of relative and absolute delay times across a network by adaptive stacking, *Geophys. J. Int.*, *157*, 332–340.

Rial, J., and V. F. Cormier (1980), Seismic waves at the epicenter's antipode, *J. Geophys. Res.*, *85*(B5), 2661–2668.

Rondenay, S., and K. M. Fischer (2003), Constraints on localized core-mantle boundary structure from multichannel, broadband SKS coda analysis, *J. Geophys. Res.*, *108*(B11), 2537, doi:10.1029/2003JB002518.

Ruigrok, E., D. Draganov, and K. Wapenaar (2008), Global-scale seismic interferometry: Theory and numerical examples, *Geophys. Prospect.*, *56*, 395–417.

Snieder, R. (2004), Extracting the Green's function from the correlation of coda waves: A derivation based on stationary phase, *Phys. Rev. E*, *69*, 1–8.

Song, X., and W. Dai (2008), Topography of Earth's inner core boundary from high-quality waveform doublets, *Geophys. J. Int.*, *175*, 386–399.

Song, X., and P. G. Richards (1996), Seismological evidence for differential rotation of the Earth's inner core, *Nature*, *382*, 221–224.

Sze, E. K. M., and R. D. van der Hilst (2003), Core mantle boundary topography from short period PcP, PKP, and PKKP data, *Phys. Earth Planet. Inter.*, *135*, 27–46.

Tanaka, S., and H. Hamaguchi (1997), Degree one heterogeneity and hemispherical variation of anisotropy in the inner core from PKP (BC)-PKP(DF) times, *J. Geophys. Res.*, *102*, 2925–2938.

Tkalčić, H. (2015), Complex inner core of the Earth: The last frontier of global seismology, *Rev. Geophys.*, *53*, 59–94, doi:10.1002/2014RG000469.

Tkalčić, H., M. Young, T. Bodin, S. Ngo, and M. Sambridge (2013), The shuffling rotation of the Earth's inner core revealed by earthquake doublets, *Nat. Geosci.*, *6*, doi:10.1038/NGEO1813.

Vidale, J. E., and P. S. Earle (2000), Fine-scale heterogeneity in the Earth's inner core, *Nature*, *404*, 273–275.

Wang, T., X. Song, and H. H. Xia (2015), Equatorial anisotropy in the inner part of Earth's inner core from autocorrelation of earthquake coda, *Nat. Geosci.*, *8*, doi:10.1038/NGEO2354.

Waszek, L., and A. Deuss (2011), Distinct layering in the hemispherical seismic velocity structure of Earth's upper inner core, *J. Geophys. Res.*, *116*, B12313, doi:10.1029/2011JB008650.

Waszek, L., J. Irving, and A. Deuss (2011), Reconciling the hemispherical structure of Earth's inner core with its super-rotation, *Nat. Geosci.*, *4*, doi:10.1038/NGEO1083.

Yao, Y., S. Whittaker, and M. S. Thorne (2015), D'' discontinuity structure beneath the North Atlantic from Scd observations, *Geophys. Res. Lett.*, *42*, 3793–3801, doi:10.1002/2015GL063989.

Yee, T. G., J. Rhie, and H. Tkalcic (2014), Regionally heterogeneous uppermost inner core observed with Hi-net array, *J. Geophys. Res. Solid Earth*, *119*, 7823–7845, doi:10.1002/2014JB011341.

Zhang, J., X. Song, Y. Li, P. G. Richards, X. Sun, and F. Waldhauser (2005), Inner core differential motion confirmed by earthquake waveform doublets, *Science*, *309*, doi:10.1126/science.1113193.